EXPERIMENTAL INVESTIGATION OF THE FLUID DYNAMICS IN WOOD COMBUSTION PROCESSES

Marc-André Baillifard, Ernesto Casartelli, Thomas Nussbaumer
University of Applied Sciences Lucerne, CH – 6048 Horw, Switzerland
www.hslu.ch

ABSTRACT: Biomass combustion is characterised by a multi step process consisting of an initial conversion of the solid fuel to gaseous compounds prior to the consecutive gas phase reactions. At combustion temperatures above 850°C, the quality of the gas phase oxidation strongly depends on the mixing quality between combustible gases and combustion air. Hence optimising the combustion chamber geometry to improve mixing and flow conditions offers a significant potential for pollutant reduction and efficiency improvement. This work shows how this optimisation can be achieved using small scale model experiments. The design process of the scaled model is presented, as well as different measurement techniques. Tracer particles are used to get a qualitative insight on the flow behaviour in the combustion chamber. The velocity in the scaled model is then measured using hot wire anemometry. Further, the mixing quality is assessed using particle tracers which are introduced in one of the flow, and by measuring their local concentration in a section of the combustion chamber. A laser is used to illuminate a planar section of the combustion chamber, and the particle concentration is recorded using a camera. This method is used to assess the mixing efficiency of two different secondary air injection configurations. In addition, the experimental results are compared with CFD calculations. Good agreement of experiment and CFD is found thus enabling a validation of critical flow regimes to improve the reliability of CFD applications.
Keywords: Combustion, emission reduction.

1 INTRODUCTION

Biomass is widely applied for energy conversion and exhibits a significant potential to replace fossil fuels [1]. However, biomass utilisation in small scale applications is related to relevant pollutant formation. The combustion is characterised by a two step process consisting of an initial conversion of the solid fuel to gaseous compounds, also called gasification products, prior to the consecutive gas phase reactions [2] The problem of wood gas combustion optimization can therefore be divided in two distinct domains: first, the solid fuel conversion and then the gas phase combustion. The solid fuel conversion is a complex process which as been addressed for instance in [3], while the present paper focuses on the gas phase combustion. As shown by [4], when the combustion temperature is above 850°C, the chemistry becomes fast, and the burnout quality is no more limited by the reaction kinetics, but by incomplete mixing and by unideal flow conditions, like for instance stratified flows. Thus, the amount of unburnt pollutants can be reduced by improved mixing and optimised combustion chamber geometry. The problem of optimising the geometry of a combustion chamber can be addressed by experiments and by modelling.

Experiments can be conducted on the real situation, or on scaled model, like it is often done in aerodynamics or in hydraulics to optimise airplanes or ship geometries. However, performing experiments on the real situation is often highly complex, when not even impossible. Furthermore, the investigation of different geometries in the real situation is very expensive and in case of combustion related to measurements at high temperatures. Model scale experiments are in this respect more flexible, and therefore more advantageous. Yet the design of a scaled model has to be carefully done, to ensure that results obtained on the scaled model are representative for the reality.

On the other hand, the increasing computational capacity in the last decades has drastically improved the modelling possibilities. Computational Fluid Dynamics (CFD) is thus nowadays widely spread and extensively used for flow optimisation in many different areas. As most of the commercial CFD codes also include several combustion modules it is also used to model the wood combustion (e.g. [5]). Nevertheless, despite all the progresses achieved in the modelling field, it is still necessary to punctually compare the modelling results to experimental ones, for validation purpose. Models and experiments are therefore two complementary optimisation methods. This work focuses on the scaled model experiments, and shows how such models can be designed.

The objective is to develop a method to investigate the fluid dynamics in wood combustion at laboratory scale models which can be used for two purposes, i.e.:

1. as a viable tool for the development of improved combustion chamber geometries, and
2. as a method to validate CFD calculations .

This work focuses on the scaled model experiments, and shows how such models can be designed so that they can be used as a viable method to develop improved combustion chamber geometries and as a tool to validate CFD calculations.

The design of scaled models requires strict conditions to be respected. These conditions and their implication are presented in the first part of this work. The actual design process is then illustrated by applying it to a grate boiler combustion chamber. The different measurements methods are also described, and finally some of the results obtained are presented, and compared with CFD calculations.

2 METHOD

As it is well known from fluid mechanics [6], scaled model experiments deliver useful results only if they fulfil similarity requirements with the reality. This is the case when the scaled model and the reality share geometric, kinematic and dynamic similarity. Geometric similarity is often quite easy to respect, even if it also means that the surface roughness has also to be scaled,

which can be sometimes quite demanding. The respect of kinematic and dynamic similarity is more challenging. From dimensional analysis [7] it is known that kinematic and dynamics similarity are fulfilled when a set of dimensionless numbers representative of the studied flow have the same value in the scaled model as in the reality. To exactly respect this condition is in most of the cases impossible, so that one has to choose which of these dimensionless parameters are most relevant. This part of the experimental model design process is crucial, because experimental results in scaled models can be misleading when important similarity criteria are not respected.

The dimensionless numbers are obtained by dimensional analysis, which is described elsewhere (for instance [7]). Here, the result of this analysis, which is the set of dimensionless numbers, is presented with a brief description of its meaning.

2.1 Reynolds number

The Reynolds number is defined as:

$$\mathrm{Re} = \frac{u \cdot L}{\nu}, \qquad \textbf{(1)}$$

where u and L are respectively a representative velocity and characteristic length of the flow, and ν is the kinematic viscosity of the fluid considered. The Reynolds number is basically a ratio between the inertial and the viscous forces in the fluid. It gives an indication of the turbulence in the flow: The greater the Reynolds number, the more turbulent the flow. For flows in a pipe, the transition between laminar and turbulent flow takes place for Reynolds numbers of 2300 [6]. As an extension, it is supposed that the transition between laminar and turbulent flows appears for similar Reynolds values in the internal flow considered here.

The Reynolds similarity is important for the problem considered here, because apart from its influence on the general flow behaviour, turbulence also plays an important role on the mixing properties of a flow.

Indeed, mixing can be seen as a process to reduce segregation between two different fluids. Segregation can be characterized by two values: the scale of segregation and the intensity of segregation [8]. The scale segregation is reduced by large scale break-up process, whereas the intensity segregation is reduced by diffusion process. Figure 1 illustrates the two segregation mechanisms. In case (a), only the scale segregation process is considered. The large scales are broken up in smaller scales, but as mixing still require diffusion of one substance in another, no actual mixing takes place. In case (b), only intensity segregation takes place. In this case, mixing occurs, but only slowly, because molecular diffusion processes are by nature slow. In case (c) intensity and scale segregation take place simultaneously. The mixing is more efficient than in case (b) because the scale segregation increases the interface between the two fluids to mix, and thus facilitates the molecular diffusion. Thus, as the large scale break-up is highly dependent on the turbulence characterized by the Reynolds number, the Reynolds number is also an important dimensionless quantity to characterize the mixing quality of two flows.

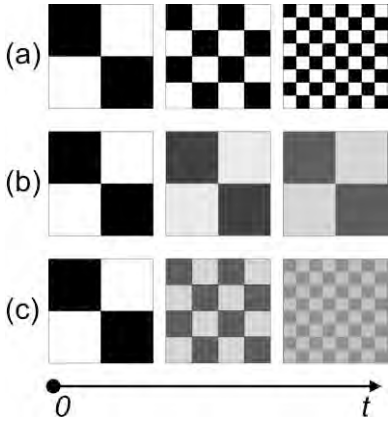

Figure 1: Illustration of the time evolution for the two segregation mechanisms: (a) Scale segregation (b) Intensity segregation (c) Intensity and scale segregation

2.2 Damköhler number

The Damköhler number is defined as:

$$Da = \frac{\tau_t}{\tau_c}, \qquad \textbf{(2)}$$

where τ_t is a flow timescale, and τ_c is a chemical timescale. As the gasification gases are mostly composed of CO [9] and as CO has a relatively slow kinetic compared to H_2 and CH_4, an estimate of the chemical timescale can be performed by considering the CO oxidation mechanism:

$$CO + OH \rightarrow CO_2 + H\,. \qquad \textbf{(3)}$$

The kinetic of this reaction can be described by [10]:

$$\frac{d[CO]}{dt} = k \cdot [CO]\,,$$

with: **(4)**

$$k = 1.3 \cdot 10^{14} \cdot [O_2]^{0.5} \cdot [H_2O]^{0.5} \cdot \exp\left(\frac{-125500}{R \cdot T}\right),$$

where $[CO]$, $[H_2O]$ and $[O_2]$ are the concentration of CO, H_2O and O_2 in mol/cm^3.

The estimation of the flow timescale can be realized in different manners. The Kolmogorov turbulence microscale could be for instance selected. This would give an information on the type of flame in the combustion chamber [11]. When the degree of oxidation in a batch process is of interest, the minimum residence time of the fuel in the combustion chamber is a good estimate. This time can roughly be estimated by:

$$\tau_t = \frac{L_{tot}}{u}, \qquad \textbf{(5)}$$

Where L_{tot} is the shortest distance between the gasification gas entrance to the combustion chamber exit, and u is the mean flow velocity in the combustion chamber. Combination of equations **(4)** and **(5)** leads to the following expression for the Damköhler number:

$$Da = \frac{\tau_t}{k}, \qquad \textbf{(6)}$$

2.3 Schmidt number

The Schmidt number is defined as:

$$Sc = \frac{\nu}{D}, \quad \textbf{(7)}$$

where D is a representative mass diffusion coefficient. The Schmidt number compares the mass diffusion effects with the momentum diffusion effects. The diffusion coefficient is the factor describing the segregation intensity [8], that is how fast the mixing at molecular level takes place. The diffusion coefficient of one gaseous substance in another can be estimated by the following formula:

$$D_{12} = \frac{1.86 \cdot 10^{-3} \cdot T^{3/2} \left(1/\tilde{M}_1 + 1/\tilde{M}_2 \right)^{1/2}}{p \cdot \sigma_{12}^2 \cdot \Omega}, \quad \textbf{(8)}$$

where T is the temperature, p the pressure, and $\tilde{M}_1$, $\tilde{M}_2$, σ_{12} and Ω are molecular properties of the two gases, which can be found in literature [12]. Finally, to determine the diffusion constant of a substance i in a mixture M, the following empirical law can be applied [11]:

$$D_i^M = \frac{1 - w_i}{\sum_{j \neq i} \frac{x_j}{D_{ij}}}, \quad \textbf{(9)}$$

Where w_i denotes the mass fraction of species i, x_j the mole fraction of the species j, and D_{ij} the binary diffusion coefficients as calculated with equation **(8)**.

Because the kinematic viscosity also increases with temperature, the Schmidt number for gases does not strongly change with temperature, and is close to 1 [12]. As illustrated in Figure 1, no mixing takes place without molecular diffusion. Thus, for the experimental model to be representative for the real scale mixing properties, Schmidt similarity is crucial.

2.4 Richardson number

The Richardson number is a dimensionless number that expresses the ratio of potential to kinetic energy. It is useful to determine if buoyancy effects are of importance when two flow of different temperature are mixed.

$$Ri = \frac{g' \cdot H}{u^2}, \quad \textbf{(10)}$$

where H is a representative height scale, and g' is the reduced gravity, as computed with the Boussinesq approximation:

$$g' = g \cdot \frac{\rho_1 - \rho_2}{\rho_{1or\,2}}, \quad \textbf{(11)}$$

where g is the gravitational acceleration, ρ_1 and ρ_2 are the densities of the two fluid flow. A small Richardson number means that buoyancy effects can be neglected. Note that the Richardson number is another expression for the Froude number: $Ri = \left(\frac{1}{Fr} \right)^{0.5}$. The Richardson number is also important in the case considered, because it shows if the density differences have to be considered or not.

2.5 The Mach number

The Mach number is the ratio between a reference velocity and the speed of sound:

$$Ma = \frac{u}{a}, \quad \textbf{(12)}$$

where a is the speed of sound in the fluid considered. The condition $Ma \leq 0.3$ ensures that compressible effects can be neglected. In the real flows considered here, this is always the case. But since downscaling is related to higher velocities, it is important to check that the incompressible hypothesis is still valid in the small scale model.

2.6 Mass Flow ratio

Finally, as the mixing of two flows is to be studied, it is clear that the mass flow rate of both flows should be of the same order of magnitude:

$$\chi = \frac{\dot{m}_1}{\dot{m}_2}, \quad \textbf{(13)}$$

where $\dot{m}_1$ (kg/s) and $\dot{m}_2$ (kg/s) are the mass flow of the two flows to be mixed.

Now that the relevant dimensionless parameters have been listed, the scaled model experiment can be designed.

3 DESIGN OF A WOOD COMBUSTION SCALED MODEL EXPERIMENT

The different steps involved in the design of a wood combustion scaled model are described for a grate boiler [13].

3.1 Description of the real scale geometry

Figure 2 shows the geometry of the combustion chamber selected for the investigated example. The main dimensions of the combustion chamber are summarized in Table A1.

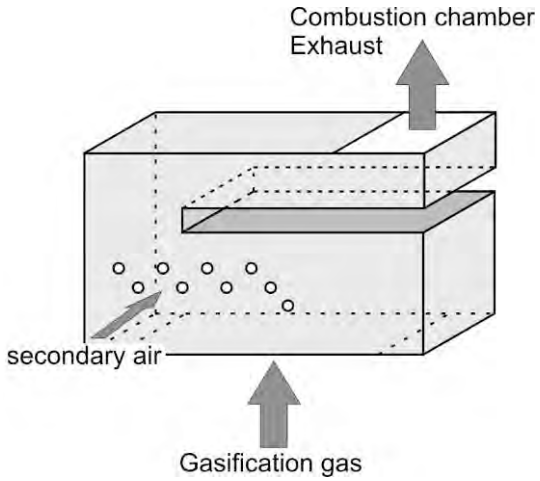

Figure 2: Schematical representation of the modelled grate boiler

Table I: Characteristics of the grate boiler

Parameter		Unit
Heat output	: $\dot{Q} = 1000$	(kW)
Combustion efficiency	: $\eta = 0.9$	(-)
Primary air ratio	: $\lambda_{prim} = 0.8$	(-)
Secondary air ration	: $\lambda_{\sec} = 1.0$	(-)
Gasification ratio	: $f = 0.9$	(-)
Wood Humidity	: $w = 0.3$	(-)
Primary air temperature	: $T_{prim} = 200$	(°C)
Secondary air temperature	: $T_{\sec} = 60$	(°C)

3.2 Value of dimensionless parameters

From the data listed in Table I the main characteristics of the flows entering the combustion chamber (i.e. velocity, temperature, viscosity, etc.) were estimated, and used to compute the dimensionless numbers listed in paragraph 2.

The Reynolds number was estimated at different sections of the combustion chamber, where the hydraulic diameter was considered as the reference length and the mean velocity as the reference speed. Three different Reynolds numbers were computed:

- The Reynolds number for the gases at the entry of the combustion chamber $\mathrm{Re}_{gasif} = 6279$
- The Reynolds number of the secondary air at the secondary air entrance: $\mathrm{Re}_{\sec} = 29886$
- The Reynolds number for the gases in the combustion chamber: $\mathrm{Re}_{comb} = 14213$

From these Reynolds, it is clear that the flow is fully turbulent.

Application of equation **(6)** to the combustion chamber considered allowed computing the Damköhler number. A value of $Da_{comb} = 2977$ is obtained, which confirms that the chemistry is much faster than the residence time of the gases in the combustion chamber.

The Richardson number for the combustion chamber is $Ri_{comb} = 0.0743$, meaning that the Buoyancy has a negligible effect on the fluid flow.

The Schmidt number was computed considering the Diffusion of CO in the gas mixture as obtained from equations **(8)** and **(9)**. The value obtained is: $Sc_{comb} = 0.79$.

The Mach number was computed at the location where the highest gas velocity is achieved, which is at the entry of the secondary air in the combustion chamber. Here, $Ma_{\sec} = 0.0414$ is obtained, which is well below 0.3, hence the flow can safely be considered as incompressible.

Finally, the mass flow ratio has a value of $\chi = 1.04$.

In summary, the high Damköhler number assures that mixing is the limiting factor, while chemistry is fast. Furthermore, the low Mach number shows that the flow is incompressible, and that given the Richardson number value of 0.0756, the buoyancy effects can be neglected. The scaled model will also need to respect the Schmidt similarity that is $Sc_{comb} = 0.79$, the mass flow ratio $\chi = 1.04$ and the Reynolds number in the combustion chamber will have to have values of about $\mathrm{Re}_{comb} = 14213$. Both, the Reynolds number of the secondary air and gasification fluxes will also have to be turbulent, and as close as possible to the values of the real boiler.

3.3 Design of the scaled model

Two additional steps are required to complete the model design. First the fluids used in the model have to be chosen, and then the scaling factor has to be fixed.

In the example considered here, the working fluid selected is air at room temperature (or at slightly elevated temperature of up to 80°C if needed) and the scaling factor chosen is 1:5. This ensures that the scaled model has a relatively small size, but with still reasonable velocities.

Considering air density and viscosity at 25°C to be $\rho_{air} = 1.184\,(\mathrm{kg/m^3})$ and $\nu_{air} = 1.56e-05$ ($\mathrm{m^2/s}$), it is possible to determine the mean flow velocity in the scaled combustion chamber from the Reynolds similarity. The mass flow ratio similarity enables then to determine the gasification and secondary air mass flow rate in the scaled model. The Mach, Richardson and Damköhler numbers can finally be computed to check that they are in the same order of magnitude than the ones from the original boiler. The different dimensionless numbers are summarized in Table II.

Table II: Dimensionless numbers of reality and scaled model

	Reality	Scaled model
Re_{gasif}	6'279	4'100
$\mathrm{Re}_{\sec}$	29'886	10'829
Re_{comb}	14'213	14'213
Sc_{comb}	0.79	0.73
$Ma_{\sec}$	0.0414	0.0282
Da_{comb}	2977	∞
Ri_{comb}	0.0743	0
χ	1.04	1.04

Both Reynolds numbers for the gasification gas and for the secondary air entry are smaller than the original ones, but still in the turbulent regime. The low Mach number also ensures that the flow is still incompressible. As already emphasised, the high Damköhler is the reason why mixing can be used as a model for combustion quality, and the low Richardson number shows that buoyancy effects can be neglected.

4 MEASUREMENT METHODS

4.1 Experimental setup

Figure 3 presents a schematic view of the experimental setup. Two ventilators are used to generate the gasification and secondary air flow. The two flow rates are measured with two differential pressure sensors, to allow regulating of the two ventilators power.

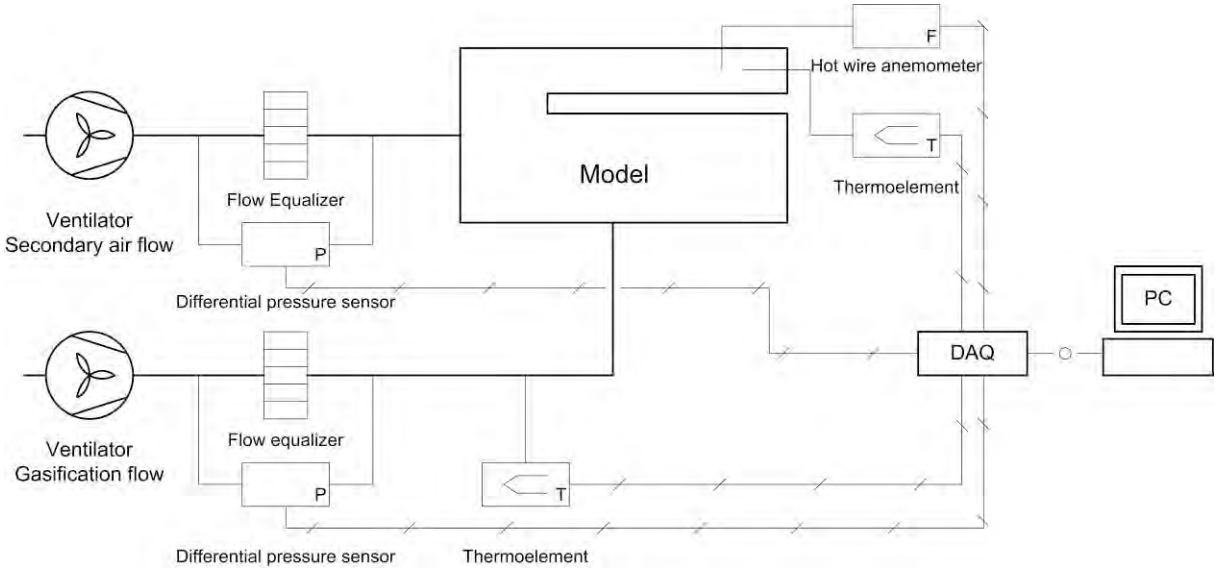

Figure 3: Schematic view of the experimental setup

When not otherwise specified, the measurements presented here were performed in two cross sections of the upper part of the combustion chamber, as illustrated in Figure 4. These two cross sections are referred to as CS1 and CS2.

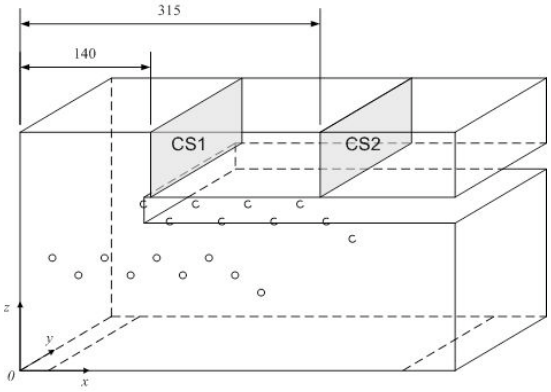

Figure 4: Schematic view of the two cross section CS1 and CS2 where measurement were performed

In order to assess the efficiency of the different measurement methods, two different variation of the combustion chamber were considered. In the first variation (Figure A2a), which is also the original one, the secondary air is injected through 18 nozzles, 9 on each side of the model. In the second variation (Figure A2b), the secondary air was injected through two large nozzles, one on each side of the model.

4.2 Velocity

For these experiments, the velocity in the section of the model was measured with help of a hot wire anemometer.

The velocities were measured in a plane, with a distance of 10 mm between two consecutive measurement points. As the hot wire anemometer is combined with a thermocouple of type K, temperature profiles were recorded simultaneously.

In a next step, Particle Image Velocimetry (PIV) will be used to receive the velocity information with a non invasive technique. This requires a more powerful laser than the one used for the mixing measurements.

4.3 Mixing quality

There are different methods to measure the mixing of twos substances, like for instance the Planar Laser Induced Florescence (PLIF) [14]. The method used here consists of seeding one of the flows with particle tracers, then illuminate a plane section of the flow with a laser sheet and analyse the repartition of the particles in this section. This method is based on the Mi-Theory [15] which states that the amount of light reflected from one position in the flow is proportional to the concentration of particle at this position. Furthermore, as shown by [16], and [17], the amount of light reflected varies linearly with the particle concentration:

$$c(x,y) = \frac{I(x,y) - I_{\min}}{I_{\max} - I_{\min}}, \qquad \textbf{(14)}$$

Where $c(x,y)$ is the local concentration of particles (per m^3), and $I(x,y)$, $I_{\max}$, $I_{\min}$ are respectively the light intensity at the point considered, and the maximal and minimal light intensity on the plane considered.

The local mixing quality $\eta(x,y)$ of two flows can be defined as difference between the particle concentration, $c(x,y)$ and the mean particle concentration of a fully mixed flow, c_{mean}. The concentration of the fully mixed fluid is defined as:

$$c_{mean} = \frac{c_{0,1} \cdot \dot{V}_1 + c_{0,2} \cdot \dot{V}_2}{\dot{V}_1 + \dot{V}_2}, \quad \textbf{(15)}$$

Where $c_{0,1}$ and $c_{0,2}$ are the initial concentrations of particles in the two non mixed flows, and $\dot{V}_1$ and $\dot{V}_2$ are their volumetric flow rate. If only the first flow is seeded with particle tracers as performed in this work,, this equation becomes:

$$c_{mean} = c_{0,1} \frac{\dot{V}_1}{\dot{V}_1 + \dot{V}_2}, \quad \textbf{(16)}$$

The local mixing quality is then defined as:

$$\eta(x,y) = \begin{cases} \dfrac{c(x,y)}{c_{mean}} & , c(x,y) \le c_{mean} \\ \dfrac{c_{0,1} - c(x,y)}{c_{0,1} - c_{mean}} & , c(x,y) > c_{mean} \end{cases}, \quad \textbf{(17)}$$

In the particular case where the two volumetric flow rates are equal, one has: $c_{0,1} = 2 \cdot c_{mean}$, and the mixing quality can be expressed by:

$$\eta(x,y) = 1 - \left| 1 - \xi(x,y) \right|, \quad \textbf{(18)}$$

Where the mixing ratio $\xi(x,y)$ was introduced. The mixing ratio is defined as:

$$\xi(x,y) = \frac{c(x,y)}{c_{mean}}, \quad \textbf{(19)}$$

Finally, the main mixing quality of a section $\overline{\eta}$ is obtained by computing the mean mixing divided by the whole plane considered:

$$\overline{\eta} = \frac{\iint \eta(x,y) \cdot dx \cdot dy}{\iint dx \cdot dy}, \quad \textbf{(20)}$$

In this experiment, the light sheet is generated by a diode laser “Magnum II 500” from StockerYale, which has a power of 375 mW at a wavelength of 680 nm. This laser has an integrated optic which allows generating a light sheet. The reflection intensity is recorded with help of a CCD camera “TM-1010” from JAI (Pulnix). This camera can record 10 bit grayscale pictures with a resolution of 1024 x 1024 pixels, at a frame rate of 15 Hz. The optic used is a 50 mm 1:1.4 objective from Cosmicar. The particles are generated using a disco fog machine “Power Fogger”, from McCrypt.

The light intensity inside the laser sheet is not perfectly uniform, due to optical effects, or to dust on the walls of the model. To compensate for this non-uniformity, a reference picture I_{ref} has to be recorded before each experiment. This reference picture is taken by only introducing the flow seeded with tracer particles in the model, to ensure a uniform particle distribution at the light sheet position. This reference picture is then used to normalize the pictures taken during the experiments. Thus, the corrected local reflection intensity is given by:

$$I'(x,y) = \frac{I(x,y)}{I_{ref}(x,y)}, \quad \textbf{(21)}$$

5 RESULTS

5.1 Qualitative flow visualisation

By filming the flow just after starting the particle seeding at transient conditions, a qualitative insight of the main flow pattern can be collected. Figure 5 shows a picture from the flow in the upper part of the combustion chamber, at cross section CS2 (See Figure 4 for exact localization). This picture shows the presence of two symmetric vortices. The presence of such vortices, also called the Dean vortices is common in flows in bended pipes, and is due to a centrifugal pressure gradient, as shown by [18].

Figure 6 shows that results of CFD computations performed on the same geometry also show the presence of these vortices. A quantitative comparison of CFD and experimental results is here not possible because the flow as it is visualized in the experimental model is the result from the transient introduction of tracer particles.

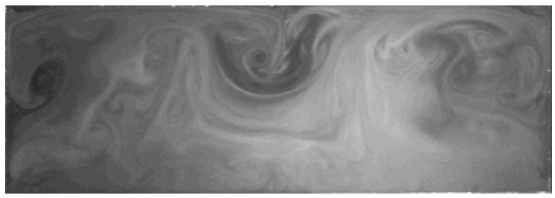

Figure 5: Qualitative flow visualization with fog particles

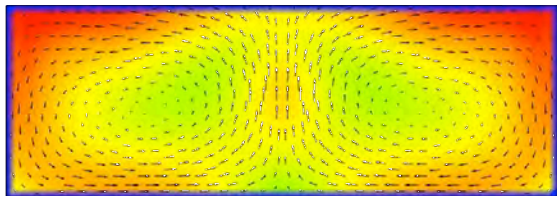

Figure 6: velocity field in the cross section of the combustion chamber.

5.2 Velocity measurements

Figure 7 shows the velocity field at cross section CS2 as measured with the hot wire anemometer. This picture shows that the velocity close to the walls is higher than at the centre, which is due to the presence of the vortices described in the preceding paragraph. Figure 8 shows the velocity field at the same location, as computed with CFD. All CFD computations presented here were performed with the CFX solver, using a SST turbulence model. Both the experimental and computed velocity fields are in good agreement.

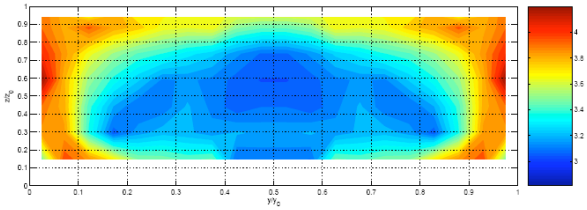

Figure 7: Velocity field measured with hot wire anemometry at CS2

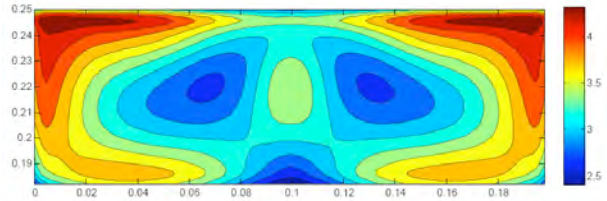

Figure 8: Velocity field at CS2 as obtained by CFD computation (CFX, SST turbulence model)

5.3 Mixing

Figure 9 shows a typical picture illustrating the repartition of the tracer particles in the cross section CS2 of the combustion chamber, when introducing the particles in the gasification air flux. Variation 2 of the model was considered here, that means the secondary air was introduced through two big holes on each side of the model.

Figure 10 shows the mixing ratio as computed from the particle concentration presented in Figure 9. The maximum and minimum mixing ratios are $\xi_{min} = 0.75$, $\xi_{max} = 1.25$, and the mean mixing efficiency at this section is $\overline{\eta} = 0.954$.

The picture from Figure 11 shows the mixing ratio at the same section, but for the first model variation V1, where the secondary air is introduced through 18 small holes in the combustion chamber. The mixing efficiency obtained is of $\overline{\eta} = 0.989$.

Due to the turbulent nature of the flow, the mixing efficiency varies with time. As done in turbulence modelling, it is possible to define the mean turbulence efficiency by averaging the time variation of the mixing efficiency. Figure 12 shows how the variation efficiency varies with time by showing the mixing efficiency computed from 150 consecutive pictures taken at a frame rate of 15 Hz, with a shutter time of 1/60 seconds. The mean mixing time is then of $\overline{\eta} = 0.938$. Proceeding in the same way for the mixing efficiency for the first variation of the model, one obtains a mixing efficiency of $\overline{\eta} = 0.986$.

Figure 9: Picture taken at CS2 showing the tracer concentration, before image processing; Model V2

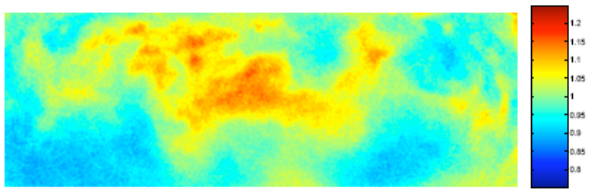

Figure 10: mixing ratio at CS2; $\xi_{min} = 0.75$, $\xi_{max} = 1.25$ $\overline{\eta} = 0.954$; Model V2

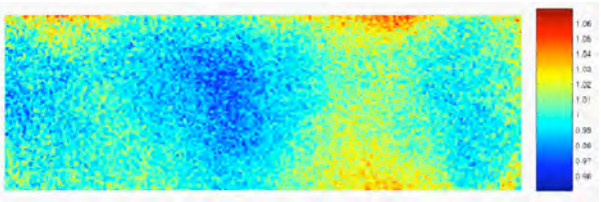

Figure 11 mixing ratio at CS2; $\xi_{min} = 0.95$, $\xi_{max} = 1.07$ $\overline{\eta} = 0.989$; Model V1

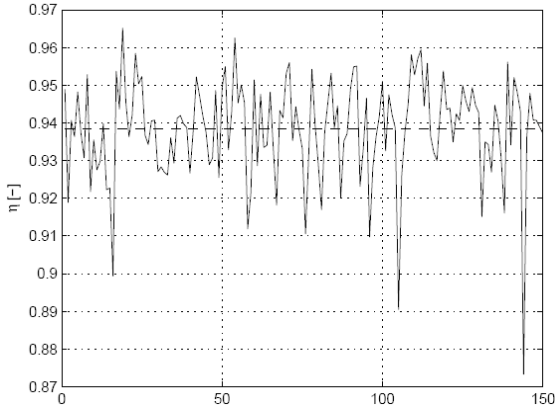

Figure 12: Variation of the mixing efficiency for 150 consecutive pictures at cross section CS2, for the Model V2. $\overline{\eta} = 0.938$

As already expected, variation 1 has a much better mixing efficiency as variation 2 of the model. This difference is due to two effects: First, the more nozzles are used for the secondary air injection, the greater is the interface between air and combustible gases. Then the area of the secondary air injection in the variation 2 of the model is 18 times larger than in the case of variation 1, which means that the inlet velocity of the secondary air is 18 times smaller in variation 2 as in variation 1, which also means that the secondary air jet penetrates less deeply in the combustion chamber, and is also less turbulent. Further investigation is needed in order to determine the respective effects of the injection speed and of the number of nozzles.

6 CONCLUSIONS

This work presents a method to design small scale model experiments for the optimisation of wood combustion chamber geometries. The dimensionless numbers relevant for wood combustion are introduced. Among others, the Reynolds number in the combustion chamber has been identified to play an important role, not only because it influences the flow pattern, but also because influences mixing.

The small scale model design process is illustrated by applying it to a generic grate boiler combustion chamber geometry. In this special case it is shown that: (i) the high Damköhler number ensures that combustion chemistry is fast and mixing is therefor the key parameter for combustion quality, (ii) due to the small Richardson number the buoyancy effects can be neglected.

Different measurement methods are presented. One method which allows a quantitative visualisation of the flow, one to directly measure the velocity repartition in a plane, and one to assess the mixing quality in a combustion chamber. These methods are easy to implement and give good results. It is for instance shown that the number of secondary air nozzles and their cross section has a great influence on the mixing quality of a given combustion chamber.

Furthermore, velocity measurements performed in the cross section of the combustion chamber are compared with CFD computation. They show a good agreement. In both cases the presence of vortices due to centrifugal pressure gradient can be seen. These vortices have a great influence on the velocity field, and their presence explains why the speed near the wall is larger than in the centre of the cross section.

In a further step, combustion chemistry is implemented in CFD, in order to investigate its influence on the main flow characteristics. The experiments on small scale model are continued to further investigate the influence of number, size, geometry, and area of secondary nozzles on the mixing efficiency for the introduced grate boiler. The experimental method will also be applied to other combustion chamber geometries, especially for small residential wood boilers. Furthermore, Particle Imaging Velocimetry (PIV) is applied, in order to facilitate velocity assessment in the model.

7 APPENDIX A

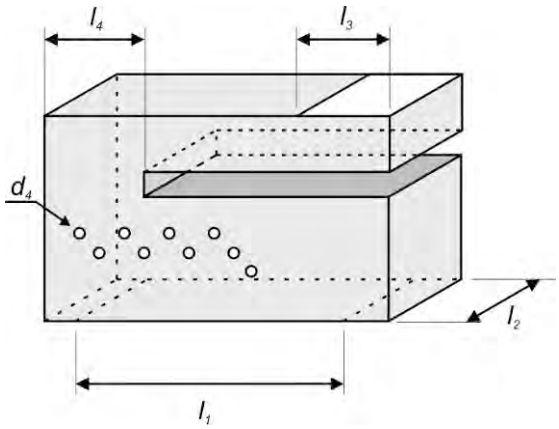

Figure A1: Geometrical description of the grate boiler analyzed

Table A1: key parameters of the grate boiler geometry, as defined in Figure A1

Symbol	Value (m)
l_1	1.855
l_2	0.989
l_3	0.740
l_4	0.649
d_1	0.0038

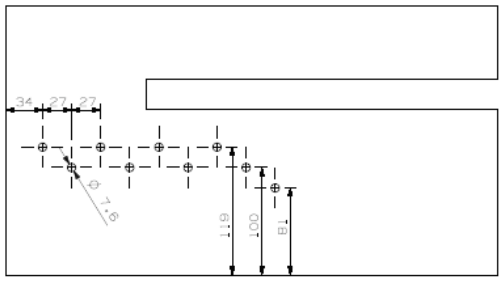

(a) Variation 1 (V1)

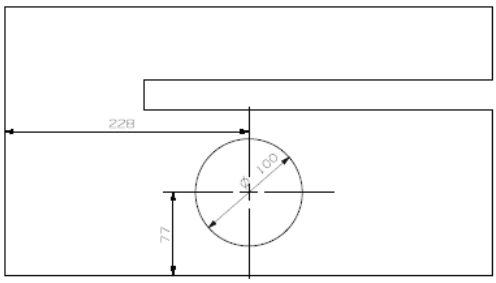

(b) Variation 2 (V2)

Figure A2 : Schematic view of two variations for the secondary air injection

8 LITERATURE

[1] Van Loo, S. and J. Koppejan, *The Handbook of Biomass Combustion and Co-firing*. 2008: Earthscan London.

[2] Nussbaumer, T., *Combustion and Co-combustion of Biomass: Fundamentals, Technologies, and Primary Measures for Emission Reduction*. Energy Fuels, 2003. **17**(6): p. 1510-1521.

[3] Bruch, C., B. Peters, and T. Nussbaumer, *Modelling wood combustion under fixed bed conditions*. Fuel, 2003. **82**: p. 729-738.

[4] Biollaz, S.M.A., T. Nussbaumer, and C. Onders, *Measuring and modelling the gas residence time.* Progress in Thermochemical Biomass Conversion, 2001. **I**: p. 573-684.

[5] Miltner, M., et al., *Process simulation and CFD calculations for the development of an innovative baled biomass-fired combustion chamber.* Applied Thermal Engineering, 2007. **27**(7): p. 1138-1143.

[6] Munson, B.R., D.F. Young, and T.H. Okiishi, *Fundamentals of fluid mechanics*. 2006: John Wiley & Sons.

[7] Szirtes, T., *Applied dimensional analysis and modeling*. 1998, New-York: McGraw Hill.

[8] Paul, E.L., V. Atiemo-Obeng, and S.M. Kresta, *Handbook of Industrial Mixing*. 2003: Wiley-IEEE. 1377.

[9] Reed, T.B., *Biomass Gasification: Principles and Technology*. Energy technology Review. Vol. 67. 1981: Noyes Data Corporation.

[10] Howard, J.B. and G.C. Williams. *Kinetics of Carbon Monoxide Oxidation in Postflamme Gases*. in *14th Symposium (Int.) on Combustion*. 1973. Combustion Institute Pittsburgh.

[11] Warnatz, J., U. Mass, and R.W. Dibble, *Combustion: Physical and Chemical Fundamentals, Modeling and Simulation, Experiments, Pollutant Formation*. 4th ed. 2006: Springer. 378.

[12] Cussler, E.L., *Diffusion*. 2nd ed. 1997: Cambridge university Press.

[13] Brzovic, T., *Methodik zur Visualisierung und Bewertung der Gasströmung in Holzfeuerungen*. 2007, ETH Zürich.

[14] Lozano, A., B. Yip, and R.K. Hanson, *Acetone: a tracer for concentration measurements in gaseous flows by planar laser-induced fluorescence.* Experiments in Fluids, 1992. **12**: p. 369-376.

[15] Modest, M.F., *Radiation Heat Transfer*. Second edition ed. 2003, San Diego: Academic Press.

[16] Gullett, B.K., P.W. Groff, and L.A. Stefanski, *Mixxing quantification by visual imaging analysis.* Experiments in Fluids, 1993. **15**: p. 443-451.

[17] Banerjee, A. and M.J. Andrews, *Statistically steady measurements of Rayleigh-Taylor mixing in a gas channel.* Physics of Fluids, 2006. **18**: p. 035107.

[18] Berger, S.A. and L. Talbot, *Flow In Curves Pipes.* Annu. Rev. Fluid Mech., 1983. **15**: p. 461-512.

Acknowledgments

- Innovation Promotion Agency (CTI)
- Liebi LNC AG, Oey-Diemtigen
- T. Rösgen, Swiss Federal Institute of Technology
- T. Brzovic, formerly Verenum and Swiss Federal Institute of Technology